Electrochemical properties of Co(OH)$_2$ powders as an anode in an alkaline battery

Yan Yao · Xiangyu Zhao · Liqun Ma ·
Tienan Qin · Meng Yang · Yi Ding

Abstract The structure and electrochemical properties of β-Co(OH)$_2$ powders, synthesized by a chemical precipitation method, were investigated. The results of X-ray diffraction show that a reversible reaction between β-Co(OH)$_2$ and hcp Co occurs. The cycling induces a capacity loss of β-Co(OH)$_2$ electrode, which is probably attributed to the dissolution of β-Co(OH)$_2$ and the subsequent formation of α-Co(OH)$_2$ and CoOOH. The results of electrochemical impedance spectra indicate that the electrochemical discharge process of the as-prepared Co(OH)$_2$ powders consists of three steps, namely the charge-transfer reactions of Co/CoH$_x$ and Co/Co(OH)$_2$, and the hydrogen diffusion within Co, depending on the depth of discharge.

Introduction

Hydrogen storage alloys have been investigated for many years due to their high-specific energy, high capacity density, and environmental advantage [1–4]. However, practical application of MH battery is limited by its low capacity and cycling stability. Many strategies, such as surface treatment, mechanical balling and elements substitution, have been extensively studied to improve the energy densities of the electrochemical battery systems [5–8]. Nevertheless, in recent years, Co and Co-based alloys have been paid considerable research attention as a promising new entry to the hydrogen storage electrode materials by virtue of their several advantages:

enhancement of electrode conductivity and charging efficiency, cycle stability and discharge capacity, and suppression of electrode swelling during charge and discharge cycling [9–12]. Chung et al. [13] studied the electrochemical hydrogenation of crystalline Co powders and found that its discharge capacity is higher than 400 mAh g^{-1}. Furthermore, the compounds of Co–B [14] and Co–P [15] have reversible electrochemical hydrogen discharge capacities of more than 300 mAh/g and good cycling stability. Moreover, many works regarding to electrochemical properties of cobalt hydroxide, used as a cathode in a nickel/metal hydride (Ni/MH) battery [16] or an electrode for an electrochemical capacitor [17], have been done. The electrochemical properties of Co(OH)$_2$ as anode materials in Ni/MH battery have not been reported.

In this study, a chemical precipitation method was used to synthesize β-Co(OH)$_2$ powders with a hexagonal structure. Changes of the structure and electrochemical properties of the β-Co(OH)$_2$ during charge and discharge cycling were investigated.

Experimental procedure

β-Co(OH)$_2$ powders, with a particle size of 100–200 nm as shown in Fig. 1, were synthesized by a chemical precipitation method. A 50 mL cobalt sulfate solution held at room temperature was added to a 50 mL potassium hydroxide solution stirred at a constant speed for 6 h. The molar ratio of KOH to CoSO$_4$ was 2:1. A pink precipitate was thoroughly rinsed with deionized water and ethanol. Finally, the sample was dried in a vacuum at 90 °C for 12 h.

The structures of the powders were analyzed by X-ray diffraction (XRD) on an ARL X'TRA diffractometer equipped with nickel filtered Cu Kα radiation. The

Y. Yao · X. Zhao · L. Ma (✉) · T. Qin · M. Yang · Y. Ding
College of Materials Science and Engineering, Nanjing
University of Technology, 5 Xinmofan Road, Nanjing,
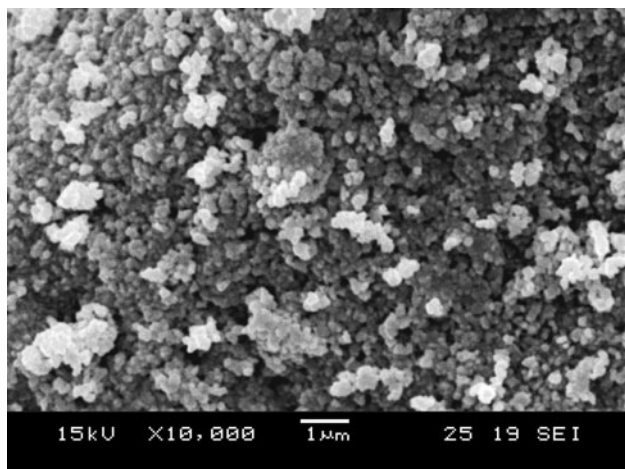Jiangsu Province 210009, China
e-mail: maliqun@njut.edu.cn

Fig. 1 Morphology of the as-prepared Co powders

morphology was observed using a JSM–5610LV scanning electron microscope (SEM).

Work electrodes were prepared by pressing 0.1 g β-Co(OH)$_2$ powders and 0.3 g Ni powders into a pellet with 10 mm in diameter and 0.4–0.6 mm in thickness, under a pressure of 15 MPa. The work electrode was charged at 60 mA/g for 6.5 h, followed by a 10 min rest and then discharged at 60 mA/g to the cut-off potential of −0.6 V (versus Hg/HgO), using BT-2000 testing equipment (Arbin, USA). Electrochemical impedance spectroscopy measurements were performed under open circuit potential in an a.c. frequency range from 5,000 to 0.001 Hz with an amplitude of 5 mV using an electrochemical working station (CHI660B, Shanghai, China). All the electrochemical tests were performed in a three-electrode cell consisting of a Ni(OH)$_2$/NiOOH counter electrode and a Hg/HgO reference electrode in a 6 M KOH solution at 298 K.

Results and discussion

Figure 2 presents the XRD patterns of the as-prepared powders. It can be verified that β-Co(OH)$_2$ (JCPDS 30-443) with a hexagonal structure is formed. The lattice parameters a and c are 3.180 and 4.629 Å, respectively. The grain size is 36.3 nm, and the unit cell volume is 40.5 Å^3.

β-Co(OH)$_2$ electrodes, containing the β-Co(OH)$_2$ powders and carbon powders at a weight ratio of 2:1, were prepared for characterizing the phase transition during charge and discharge testing. Figure 3 shows the XRD patterns of the β-Co(OH)$_2$ powders as a function of charge and discharge. A phase transition from Co(OH)$_2$ to Co occurs during charge testing. However, all diffraction peaks of Co disappear and the intensities of the diffraction peaks corresponding to β-Co(OH)$_2$ are obviously increase after discharge. Hence, it can be confirmed that the
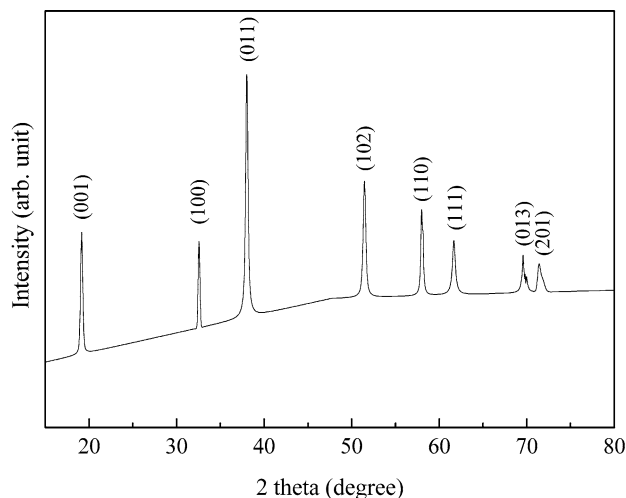

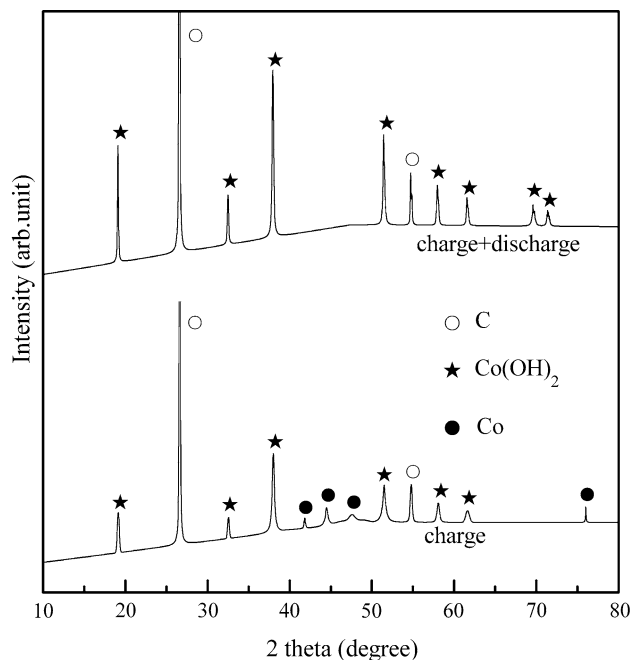Fig. 2 XRD patterns of the as-prepared Co(OH)$_2$ powders

Fig. 3 XRD patterns of the Co(OH)$_2$ powders as a function of charge and discharge

reversible phase transition of Co/Co(OH)$_2$ is the dominant reaction during charge and discharge processes.

Figure 4 shows the electrochemical charge and discharge curves of the β-Co(OH)$_2$ electrodes at a current of 60 mA g^{-1} during the first, the second, and the third cycles. Two stages for the β-Co(OH)$_2$ electrode can be observed regarding the charge process. A long plateau at about −900 mV versus Hg/HgO appears in the first stage. This plateau can be principally attributed to the phase transformation from Co(OH)$_2$ to Co, as confirmed by the results shown in Fig. 3. However, the small figure embedded in Fig. 4, shows an interesting phenomenon at the beginning of
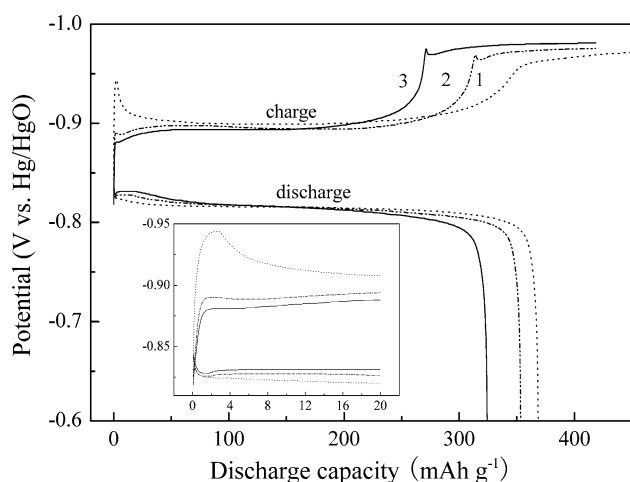
Fig. 4 Charge and discharge curves of the $Co(OH)_2$ electrodes at a current density of 60 mA g^{-1} during several cycles

Fig. 5 Discharge curve of $Co(OH)_2$ electrode at a discharge current density of 60 mA g^{-1}

the first charge process, in which the potential first decreases and then increases. The occurrence of this phenomenon may be due to the reaction rate of $Co(OH)_2$ to Co is slower than the rate of hydrogen adsorption at first. The hydrogen adsorbed on the particle surface leads to a decrease in the potential. Subsequently, part of $Co(OH)_2$ transforms to Co, which absorbs the hydrogen adsorbed on the surface, resulting in an increase of the potential of the electrode. This phenomenon does not occur during the other cycles. This may be attributed to a faster transformation from $Co(OH)_2$ to Co after the first charge/discharge process. The followed drastic decrease in potential may be related to a saturation of Co hydride and the finish of the phase transition. Finally, hydrogen evolution reaction occurs. On the other hand, there is only one plateau appearing in the discharge curves around −850 mV versus Hg/HgO. Elumalai et al. [16] found that the potential of a $Co(OH)_2$ negative electrode remains nearly constant at about –0.8 V during the course of discharge in a galvanic cell. Hence, the discharge capacities are mainly attributed to the reaction of Co to $Co(OH)_2$. It can be seen from the discharge curves that the discharge plateau becomes narrow and a capacity loss appears as the cycle number increases. The reasons will be explained in detail in the next section.

Figure 5 shows the discharge capacities of the β-$Co(OH)_2$ electrodes as a function of cycle number. It can be seen that the discharge capacity of the β-$Co(OH)_2$ electrode reaches a maximum at the first cycle without any activation and then depresses gradually with the cycle number increasing. This may relate to the dissolution and precipitation of $Co(OH)_2$ in the alkaline electrolyte. Haran et al. [18] mentioned that the $Co(OH)_2$ could be oxidized to $HCoO_2^-$ in an alkaline electrolyte, which could be subsequently precipitated into $Co(OH)_2$. In order to further identify the precipitation, SEM and XRD were carried out to characterize the structure and morphology of the precipitation. Figures 6 and 7 show the
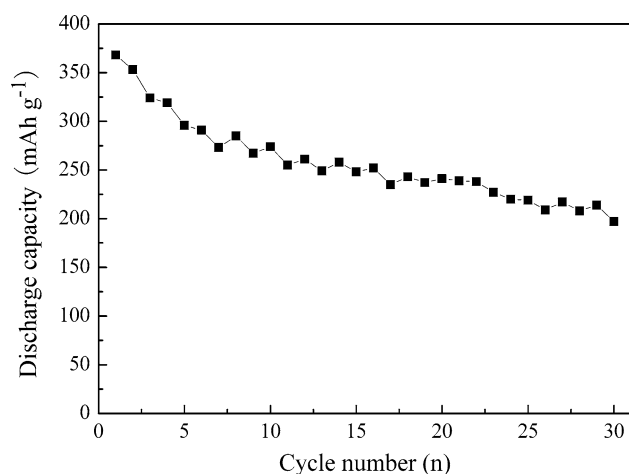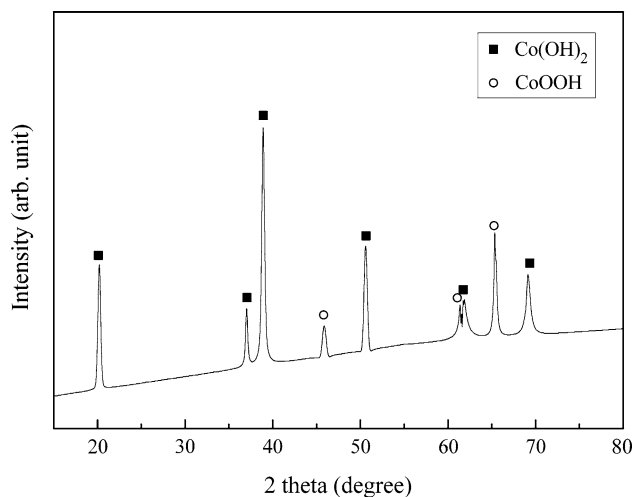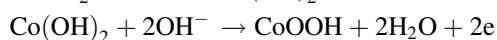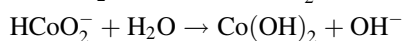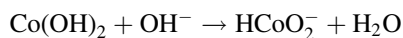

Fig. 6 XRD pattern of the precipitation

SEM image and the XRD pattern, respectively. The result of the XRD pattern demonstrates that the precipitation sample on the inner surface of the glass pipe mainly consists of α-$Co(OH)_2$ coexisting a little CoOOH. The reaction mechanism of the precipitation can be primarily expressed as follows [18, 19],

$$Co(OH)_2 + OH^- \rightarrow HCoO_2^- + H_2O$$
$$HCoO_2^- + H_2O \rightarrow Co(OH)_2 + OH^-$$
$$Co(OH)_2 + 2OH^- \rightarrow CoOOH + 2H_2O + 2e$$

When the β-$Co(OH)_2$ electrode are immersed into a 6 M KOH electrolyte for charge and discharge testing, a little part of β-$Co(OH)_2$ are decomposed and oxidized to $HCoO_2^-$, which could be subsequently precipitated into α-$Co(OH)_2$ in the KOH alkaline solution. A small fraction of α-$Co(OH)_2$ could be further transformed into CoOOH. The SEM image shows that the precipitation exhibits a
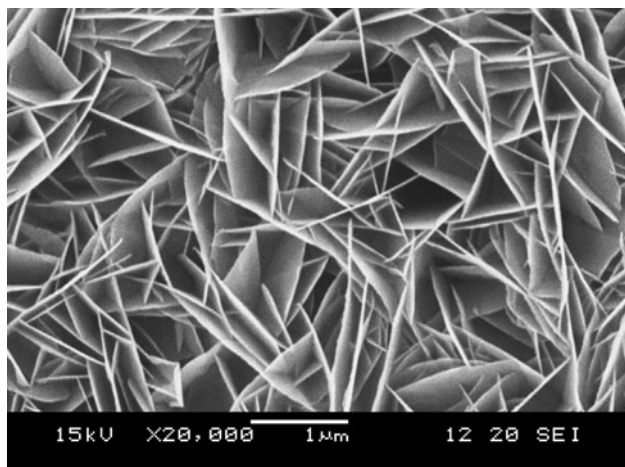
Fig. 7 SEM image of the precipitation

nano-flake structure, which is similar to the results from Kong et al. [17] and Hosono et al. [20].

In order to further confirm the electrochemical reaction mechanism of the β-Co(OH)$_2$ electrode, the electrochemical impedance spectra (EIS) was conducted to investigate the electrochemical discharge process of the as-prepared β-Co(OH)$_2$ electrode during charge and discharge testing, considering various depths of discharge (DODs). Figure 8 shows the EIS patterns of the β-Co(OH)$_2$ electrodes fully activated. It is clear that each EIS spectrum consists of three semicircles. This is in accord with the result from the Bode-phase plots, as shown in Fig. 8b. The semicircle in the high-frequency region is attributed to the contact resistance between the alloy particles and the current collector. The subsequent semicircle in the middle–frequency region is related to a charge-transfer process at the electrode/electrolyte interface, which is likely due to the reaction of Co/CoH$_x$. It is evident that the reaction resistance of Co/CoH$_x$ increases by increasing the DOD. This is ascribed to the decrease of active Co on the electrode surface. The third semicircle in the low frequency region corresponds to the charge-transfer reaction resistance of Co/Co(OH)$_2$. Furthermore, when the DOD is 0%, a short line following the semicircle caused by the reaction of Co/Co(OH)$_2$ reflects the hydrogen diffusion within Co. However, this short line cannot be found for the electrodes at 50% and 90% DODs. At the initial discharge stage, the high hydrogen concentration in the bulk electrode restricts the mobility of hydrogen atoms [21] and, consequently, the hydrogen desorption is controlled by a mixed limiting-step of the charge-transfer and hydrogen diffusion. With the increase in DOD, the active Co on the sample surface is gradually oxidized to Co(OH)$_2$ and, thus, the charge-transfer reaction of hydrogen desorption is limited, resulting in a transformation of the controlling-step from the mixed rate-determining process at the initial discharge
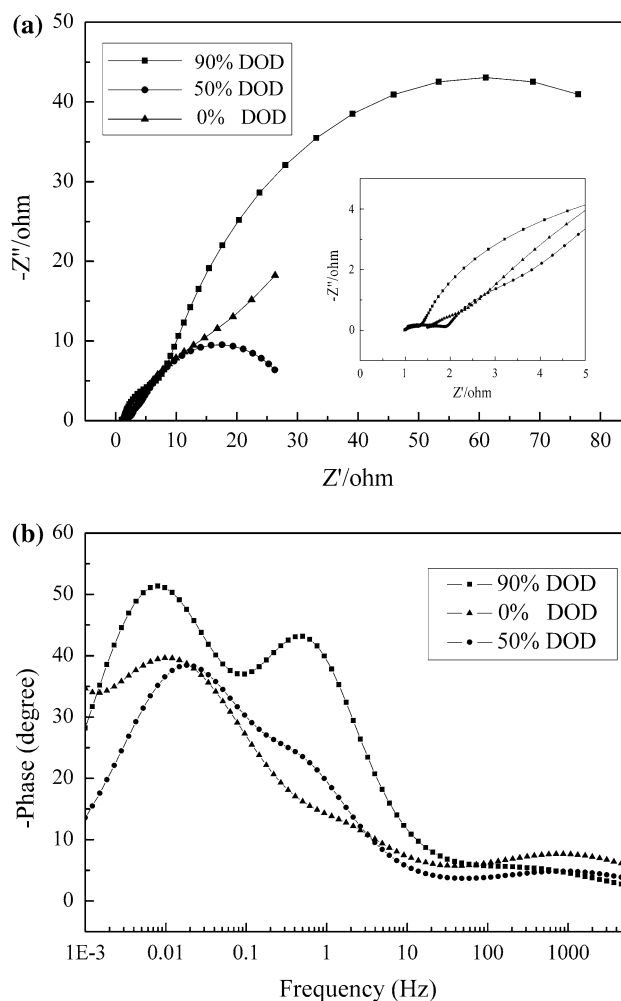

Fig. 8 EIS patterns of the as-prepared Co(OH)$_2$ electrodes: **a** Nyquist plots and **b** Bode-phase plots

stage to the charge-transfer reaction of Co/Co(OH)$_2$ and/or Co/CoH$_x$ at the final discharge stage.

Conclusion

The Co(OH)$_2$ powders were synthesized by means of a chemical precipitation method. The structure and hydrogen storage characteristics have been investigated. It is found, by XRD analysis, that the as-prepared Co(OH)$_2$ powders consist of β-Co(OH)$_2$ phase with a hexagonal structure. A reversible reaction between β-Co(OH)$_2$ and hcp Co occurs during charge and discharge testing. The chemical reactions of β-Co(OH)$_2$/HCoO$_2^-$, HCoO$_2^-$/α-Co(OH)$_2$, and α-Co(OH)$_2$/CoOOH in KOH solution during charge and discharge testing induce a capacity loss. The results of EIS show that the electrochemical discharge process of the as-prepared Co(OH)$_2$ electrode consists of three steps, namely the charge-transfer reaction of Co/Co(OH)$_2$, the

hydrogen diffusion within Co, and the charge-transfer reaction of Co/CoH$_x$. The controlling-step of the electrochemical processes transforms from a mixed rate-determining process containing the charge-transfer of Co/Co(OH)$_2$ and/or Co/CoH$_x$ and hydrogen diffusion at the initial discharge stage to the charge-transfer reaction of Co/Co(OH)$_2$ and/or Co/CoH$_x$ at the final discharge stage.

References

1. Hu WK, King DM, Jeon SW, Lee JY (1998) J Alloy Compd 270:255
2. Kohno T, Yoshida H, Kawashima F, Inaba T, Sakai I, Yamamoto M, Kanda M (2003) J Alloy Compd 311:L5
3. Chen WX (2000) J Power Sour 90:201
4. Zhao XY, Ma LQ, Ding Y, Shen XD (2009) Int J Hydrogen Energy 34:3389
5. Cui N, He P, Luo JL (1999) Acta Mater 47:3737
6. Zhao XY, Ma LQ, Gao YJ, Ding Y, Shen XD (2009) Int J Hydrogen Energy 34:1904
7. Wang Y, Wang X, Gao XP, Shen PW (2008) Mater Chem Phys 110:234
8. Miao H, Pan HG, Zhang SC, Chen N, Li R, Gao MX (2007) Int J Hydrogen Energy 32:3387
9. Rune S (2000) J Power Sour 90:153
10. Pralong V, Chabre Y, Delahaye-Vidal A, Tarascon JM (2002) Solid State Ionics 147:73
11. Chen SR, Wang KW, Teng MH, Perng TP (2009) Int J Hydrogen Energy 34:1383
12. Mao LC, Tong JY, Shan ZQ, Yin SH, Wu F (1999) J Alloys Compd 293–295:829
13. Chung SR, Wang KW, Perng TP (2006) J Electrochem Soc 153:A1128
14. Wang YD, Ai XP, Yang HX (2004) Chem Mater 16:5194
15. Cao YL, Zhou WC, Li XY, Ai XP, Gao XP, Yang HX (2006) Electrochim Acta 51:4285
16. Elumalai P, Vasan HN, Munichandraiah N (2001) J Power Sour 93:201
17. Kong LB, Lang JW, Liu M, Luo YC, Kang L (2009) J Power Sour 194:1194
18. Haran BS, Popov BN, White RE (1998) J Electrochem Soc 145:3000
19. Simpraga RP (1993) J Electroanal Chem 355:79
20. Hosono E, Fujihara S, Honma I, Ichihara M, Zhou HS (2006) J Power Sour 158:779
21. Zhao XY, Ma LQ, Yang M, Ding Y, Shen XD (2010) Int J Hydrogen Energy 35:3077